Table 3 Blood chemistry of chimeric, uPA/SCID, and uPA (wt/wt)/SCID mice

Sex		Chimeric		uPA/SCID	SCID	Human (reference value,
		Male	Female	Male	Male	Male and female)
Age (w)		13.4 ± 0.9	12.0 ± 1.9	12.0 ± 0.0	11.0 ± 0.0	—
Body weight		17.3 ± 2.3	17.6 ± 1.7	17.4 ± 0.3	27.3 ± 0.9	—
n		*5*	*5*	*5*	*3*	—
GOT	U/l	214.6 ± 75.1**[a]	126.8 ± 72.5	367.6 ± 107.7**[b]	44.0 ± 23.3	20–48[c]
GPT	U/l	98.6 ± 16.8*[a]	58.6 ± 18.0	176.4 ± 28.9**[b]	44.3 ± 37.7	10–40[c]
GGT	U/l	23.0 ± 4.6**[a]	15.0 ± 3.9	1.2 ± 0.4	3.7 ± 4.6	0–30[c]
CHE	U/l	396.8 ± 80.2**[a]	282.2 ± 34.1	42.6 ± 8.0**[b]	18.0 ± 5.2	660–1620[d]
BUN	mg/dl	27.3 + 4.0	23.2 ± 4.6	24.6 ± 9.1	25.3 ± 3.9	8–23[c]
TCHO	mg/dl	88.0 ± 25.8	69.6 ± 18.7	56.8 ± 6.8**[b]	83.3 ± 2.5	< 200[c]
HDL-c	mg/dl	20.2 ± 3.4**[a]	18.8 ± 3.7	52.4 ± 7.0**[b]	72.7 ± 6.8	35–80[c]
TG	mg/dl	129.2 ± 24.6	133.2 ± 13.8	82.2 ± 11.0	99.3 ± 10.2	10–190[c]
TBIL	mg/dl	0.4 ± 0.1	0.4 ± 0.0	0.5 ± 0.2	0.6 ± 0.5	0.3–1.2[c]
GLU	mg/dl	154.6 ± 21.6	148.8 ± 31.9	116.4 ± 30.5	154.7 ± 14.2	70–110[c]
ALB	g/dl	3.0 ± 0.4*[a]	2.4 ± 0.1	1.7 ± 0.3	2.2 ± 0.3	3.5–5.0[c]
TP	g/dl	5.0 ± 0.7	4.2 ± 0.3	3.5 ± 0.7*[c]	5.3 ± 0.6	6.0–8.0[c]

[a] Chimeric mouse (male) *vs* SCID mouse (male).
[b] uPA/SCID mouse (male) *vs* SCID mouse (male).
[c] Reference number.[21]
[d] Reference number.[22]
*$P < 0.05$, **$P < 0.01$.

because of species differences. For example, h-heps were considered to be deficient in growth hormone (GH) because the hGH receptor (hGHR) was unresponsive to mouse GH.[26] Human insulin-like growth factor 1 (IGF-1) was undetectable in chimeric mouse sera.[17,27] We recently identified 4 downregulated and 14 upregulated genes in the chimeric mouse livers when they were treated with hGH.[17] In this microarray analysis, the expression level of fatty acid desaturase 1 (FADS1, c-heps/h-heps ratio: 20.225) was significantly higher in c-hep than in h-heps (Supplementary Table 3). Meanwhile, the expression levels of IGF-1 (c-heps/h-heps ratio: 0.002), suppressors of cytokine signaling 2 (SOCS2; 0.012 and 0.030), nicotinamide *N*-methyltransferase (NNMT; 0.025 and 0.019) chromosome 5 open reading frame 13 (C5orF13; 0.345), solute carrier family 16, member 1(SLC16A1; 0.485 and 0.432), steroid-5-α-reductase, and α-polypeptide 1 (SRD5A1; 0.486 and 0.461) were significantly lower in c-heps (Supplementary Table 3). Consequently, 1 of 170 genes and 6 of 320 genes were up- and down-regulated in c-heps, respectively, because of the lack of hGH in the sera.

Biochemical testing of the chimeric mouse sera revealed high GOT and GPT levels in chimeric and uPA/SCID mice, probably because of m-hep damage caused by uPA expression.[2,28] CHE was higher in chimeric mice than in uPA/SCID and SCID mice, which may be a result of the influence of typically higher h-hep CHE levels. Serum HDL-c levels are higher in mice than in humans, because mice lack cholesterol ester transport proteins that convert HDL-c to LDL-c.[29] HDL-c was lower in the chimeric mice than in the uPA/SCID mice, SCID mice, and humans. At present, the reason for the low HDL-c levels in the chimeric mice is not clear. Further investigations are needed to resolve this question.

We conclude that the chimeric mouse livers showed nearly normal morphology and expressed most genes at similar levels as normal human livers.

Supplementary Information accompanies the paper on the Laboratory Investigation website (http://www.laboratoryinvestigation.org)

ACKNOWLEDGEMENTS
A part of this research was supported by the Yoshizato Project of the Cooperative Link of Unique Science and Technology for Economic Revitalization (CLUSTER), Japan. We thank Y Yoshizane and R Inoue from PhoenixBio, and H Kohno, Y Matsumoto, and S Nagai from CLUSTER for their technical assistance. We also thank H Duimel, University Maastricht, for preparation of the SEM specimen.

DISCLOSURE/CONFLICT OF INTEREST
The authors declare no conflict of interest.

1. Dalvie D, Obach RS, Kang P, *et al.* Assessment of three human in vitro systems in the generation of major human excretory and circulating metabolites. Chem Res Toxicol 2009;22:357–368.

2. Tateno C, Yoshizane Y, Saitou N, *et al.* Near completely humanized liver in mice shows human-type metabolic responses to drugs. Am J Pathol 2004;165:901–912.
3. Katoh M, Matsui T, Okamura H, *et al.* Expression of human phase II enzymes in chimeric mice with humanized liver. Drug Metab Dispos 2005;33:1333–1340.
4. Nishimura M, Yoshitsugu H, Yokoi T, *et al.* Evaluation of mRNA expression of human drug-metabolising enzymes and transporters in chimeric mouse with humanized liver. Xenobiotica 2005;35: 877–890.
5. Shi J, Fujieda H, Kokubo Y, *et al.* Apoptosis of neutrophils and their elimination by Kupffer cells in rat liver. Hepatology 1996;24: 1256–1263.
6. Warren A, Le Couteur DG, Fraser R, *et al.* T lymphocytes interact with hepatocytes through fenestrations in murine liver sinusoidal endothelial cells. Hepatology 2006;44:1182–1190.
7. Sato Y, Yamada H, Iwasaki K, *et al.* Human hepatocytes can repopulate mouse liver: histopathology of the liver in human hepatocyte-transplanted chimeric mice and toxicologic responses to acetaminophen. Toxicol Pathol 2008;36:581–591.
8. Meuleman P, Libbrecht L, De Vos R, *et al.* Morphological and biochemical characterization of a human liver in a uPA-SCID mouse chimera. Hepatology 2005;41:847–856.
9. Nonaka H, Tanaka M, Suzuki K, *et al.* Development of murine hepatic sinusoidal endothelial cells characterized by the expression of hyaluronan receptors. Dev Dyn 2007;236:2258–2267.
10. Katayama S, Tateno C, Asahara T, *et al.* Size-dependent in vivo growth potential of adult rat hepatocytes. Am J Pathol 2001;158: 97–105.
11. Ban D, Kudo A, Sui S, *et al.* Decreased Mrp2-dependent bile flow in the after-warm ischemic rat liver. J Surg Res 2009;153:310–316.
12. Mabuchi A, Wake K, Marlini M, *et al.* Protection by glycyrrhizin against warm ischemia-reperfusion-induced cellular injury and derangement of the microcirculatory blood flow in the rat liver. Microcirculation 2009;16:364–376.
13. Wisse E, Braet F, Duimel H, *et al.* Fixation methods for electron microscopy of human and other liver. World J Gastroenterol 2010;16:2851–2866.
14. Seglen PO. Preparation of isolated rat liver cells. Methods Cell Biol 1976;13:29–83.
15. Bolstad BM, Irizarry RA, Astrand M, *et al.* A comparison of normalization methods for high density oligonucleotide array data based on variance and bias. Bioinformatics 2003;19:185–193.
16. Eisen MB, Spellman PT, Brown PO, *et al.* Cluster analysis and display of genome-wide expression patterns. Proc Natl Acad Sci USA 1988;95:14863–14868.
17. Tateno C, Kataoka M, Utoh R, *et al.* Growth hormone-dependent pathogenesis of human hepatic steatosis in a novel mouse model bearing a human hepatocyte-repopulated liver. Endocrinology 2011;152:1479–1491.
18. Asahina K, Sato H, Yamasaki C, *et al.* Pleiotrophin/HB-GAM as a mitogen of rat hepatocytes and its role in regeneration and development of liver. Am J Pathol 2002;160:2191–2205.
19. Benjamini Y, Hochberg Y. Controlling the false discovery rate: a practical and powerful approach to multiple testing. J Roy Statist Soc Ser B 1995;57:289–300.
20. Utoh R, Tateno C, Kataoka M, *et al.* Hepatic hyperplasia associated with discordant xenogeneic parenchymal-nonparenchymal interactions in human hepatocyte-repopulated mice. Am J Pathol 2010;177:654–665.
21. Michael L. Laboratory Medicine: The Diagnosis in the Clinical Laboratory, New York, 2010.
22. Jensen FS, Skovgaard LT, Viby-Mogensen J. Identification of human plasma cholinesterase variants in 6,688 individuals using biochemical analysis. Acta Anaesthesiol Scand 1995;39:157–162.
23. Porter RK, Brand MD. Causes of differences in respiration rate of hepatocytes from mammals of different body mass. Am J Physiol 1995;269:R1213–R1224.
24. Maeno H, Ono T, Dhar DK, *et al.* Expression of hypoxia inducible factor-1alpha during liver regeneration induced by partial hepatectomy in rats. Liver Int 2005;25:1002–1009.
25. Tomoyori T, Ogawa K, Mori M, *et al.* Ultrastructural changes in the bile canaliculi and the lateral surfaces of rat hepatocytes during restorative proliferation. Virchows Arch B Cell Pathol Incl Mol Pathol 1983;42: 201–211.
26. Souza SC, Frick GP, Wang X, *et al.* A single arginine residue determines species specificity of the human growth hormone receptor. Proc Natl Acad Sci USA 1995;92:959–963.
27. Masumoto N, Tateno C, Tachibana A, *et al.* GH enhances proliferation of h-heps grafted into immunodeficient mice with damaged liver. J Endoclinol 2007;194:529–537.
28. Sandgren EP, Palmiter RD, Heckel JL, *et al.* Complete hepatic regeneration after somatic deletion of an albumin-plasminogen activator transgene. Cell 1991;66:245–256.
29. Dinchuk J, Hart J, Gonzalez G, *et al.* Remodelling of lipoproteins in transgenic mice expressing human cholesteryl ester transfer protein. Biochim Biophys Acta 1995;1255:301–310.

CLINICAL REPORT

AMERICAN JOURNAL OF medical genetics PART A

Expression Analysis of a 17p Terminal Deletion, Including *YWHAE*, but not *PAFAH1B1*, Associated With Normal Brain Structure on MRI in a Young Girl

Keisuke Enomoto,[1,2] Yasuhiro Kishitani,[1] Makiko Tominaga,[1] Aki Ishikawa,[1] Noritaka Furuya,[1] Noriko Aida,[3] Mitsuo Masuno,[4] Ken-Ichiro Yamada,[5] and Kenji Kurosawa[1,6]*

[1]Division of Medical Genetics, Kanagawa Children's Medical Center, Yokohama, Japan

[2]Department of Pediatrics and Developmental Biology, Tokyo Medical and Dental University Graduate School of Medical and Dental Science, Tokyo, Japan

[3]Department of Radiology, Kanagawa Children's Medical Center, Yokohama, Japan

[4]Genetic Counseling Program, Graduate School of Health and Welfare, Kawasaki University of Medical Welfare, Yokohama, Japan

[5]Department of Pediatrics, Hiratsuka City Hospital, Hiratsuka, Japan

[6]Kanagawa Children's Medical Center, Institue for Clinical Research, Yokohama, Japan

Manuscript Received: 28 September 2011; Manuscript Accepted: 1 June 2012

Tyrosine 3-monooxygenase/tryptophan 5-monooxygenase activation protein, epsilon polypeptide (*YWHAE*), on chromosome 17p13.3, has been shown to play a crucial role in neuronal development. The deletion of *YWHAE*, but not platelet-activating factor acetylhydrolase, isoform 1b, subunit 1 (*PAFAH1B1*), underlies a newly recognized neurodevelopmental disorder, characterized by significant growth retardation, developmental delay/intellectual disability (DD/ID), distinctive facial appearance, and brain abnormalities. Here, we report on a girl with a terminal deletion of 17p13.3, including *YWHAE* but not *PAFAH1B1*, showing normal brain structure on MRI. She had mild developmental delay, a distinctive facial appearance, and severe growth retardation despite normal growth hormone levels, which was improved by growth hormone therapy. Expression analysis of *YWHAE* and *PAFAH1B1* yielded results consistent with array CGH and FISH results. These results indicate that the dosage effect of *YWHAE* varies from severe to very mild structural brain abnormalities, and suggest that the expression of *YWHAE* is associated with a complex mechanism of neuronal development. © 2012 Wiley Periodicals, Inc.

Key words: *YWHAE*; *PAFAH1B1*; microdeletion 17p13.3; growth retardation

How to Cite this Article:
Enomoto K, Kishitani Y, Tominaga M, Ishikawa A, Furuya N, Aida N, Masuno M, Yamada K-I, Kurosawa K. 2012. Expression analysis of a 17p terminal deletion, including *YWHAE*, but not *PAFAH1B1*, associated with normal brain structure on MRI in a young girl.
Am J Med Genet Part A 158A:2347–2352.

INTRODUCTION

Deletions of 17p13.3 result in the neuronal migration disorders including lissencephaly and variable structural disorders of the brain [Dobyns et al., 1993]. Haploinsufficiency of platelet-activating factor acetylhydrolase, isoform 1b, subunit 1 (*PAFAH1B1*) and tyrosine 3-monooxygenase/tryptophan 5-monooxygenase activation protein, epsilon polypeptide (*YWHAE*), genes located in this region, are responsible for Miller–Dieker syndrome, which is characterized by lissencephaly, distinctive facial appearance, and severe neurological dysfunctions [Cardoso et al., 2003].

Recently, it has been shown that patients with deletion of *YWHAE*, but not *PAFAH1B1*, have significant growth retardation, developmental delay/intellectual disability (DD/ID), distinctive facial appearance, and brain abnormalities [Nagamani et al., 2009; Bruno et al., 2010; Mignon-Ravix et al., 2010; Schiff et al., 2010; Shimojima et al., 2010; Tenney et al., 2011]. These results indicated that the *YWHAE* plays a crucial role in neuronal development [Toyo-oka et al., 2003]. The structural abnormalities

---

Additional supporting information may be found in the online version of this article.

Grant sponsor: The Ministry of Health, Labour and Welfare of Japan.

*Correspondence to:
Kenji Kurosawa, M.D., Ph.D., Division of Medical Genetics, Kanagawa Children's Medical Center, 2-138-4 Mutsukawa, Minami-ku, Yokohama 232-8555, Japan. E-mail: kkurosawa@kcmc.jp

Article first published online in Wiley Online Library (wileyonlinelibrary.com): 7 August 2012

DOI 10.1002/ajmg.a.35542

© 2012 Wiley Periodicals, Inc.

observed in the brain and cognitive deficiency present in these patients is variable. Recently much attention has been given to the genotype–phenotype correlations based on the breakpoints distal to *PAFAH1B1* in 17p13.3 [Bi et al., 2009].

Here, we report on the case of a girl with mild developmental delay but normal brain structure on MRI, with a terminal deletion of 17p13.3 that involved *YWHAE*, but not *PAFAH1B1*, as demonstrated by FISH and gene expression studies. These results imply that YWHAE is associated with a complex mechanism of neuronal development.

CLINICAL REPORT

The 5-year-old girl was born at 40 weeks of gestation by cesarean due to fetal distress, to healthy, non-consanguineous parents. The father and mother were 34 and 33 years old, respectively, and previously had a healthy son. There was no family history of epilepsy and intellectual disability. The girl's birth weight was 2,156 g, length 46 cm, and occipito-frontal circumference (OFC) 33.6 cm, respectively. Her Apgar scores were 6/8. She was hospitalized for severe congenital anemia, caused by feto-maternal transfusion syndrome, and persistent pulmonary hypertension of the newborn.

Developmental milestones were mildly delayed; head control was achieved by 4 months, sitting by 8 months, walking by 18 months, single word by first year, and two-word phrase by 2 years. At 3 years, a ligation procedure for the patent ductus arteriosus was performed. The developmental quotient (DQ), using the Kyoto Scale for Psychological Development, was 70 at the age of 4 years and 9 months. At this age, she presented febrile convulsion lasting 1 min. Biochemical analysis revealed normal levels of insulin-like growth factor-1 (IGF-1), basal growth hormone (GH), thyroid function, cortisol, adrenocorticotropic hormone (ACTH), and prolactin. GH levels in response to stimulation tests were normal for her age. However, growth hormone therapy was started from the age of 4 years as growth retardation had been noted from infancy; this was effective to achieve catch-up growth. Standard karyotyping was normal.

On examination at the age of 5 years, her height was 97.5 cm (−2.4 SD), weight 14.1 kg (−1.5 SD), and OFC 51.4 cm (+0.6 SD). Her facial appearance was distinctive characterized by macrocephaly, a high forehead, hypertelorism, and thin upper lip vermilion (Fig. 1). Brain MRI at 3 T showed almost normal appearances without any structural abnormality but faint patchy high-intensity areas in the frontal subcortical white matter on T2-weighted and fluid attenuated inversion recovery (FLAIR) images (Fig. 2).

MATERIALS AND METHODS

Written informed consent was obtained from the parents of the patient in accordance with the Kanagawa Children's Medical Center Review Board and Ethics Committee.

Molecular Cytogenetic and Array CGH Investigations

An initial FISH analysis for patients with DD/ID and/or multiple congenital anomalies (MCA) was carried out with subtelomeric probes (Vysis, Downers Grove, IL) according to the standard protocol. A probe specific for Miller–Dieker syndrome (LIS1; Vysis) was also used.

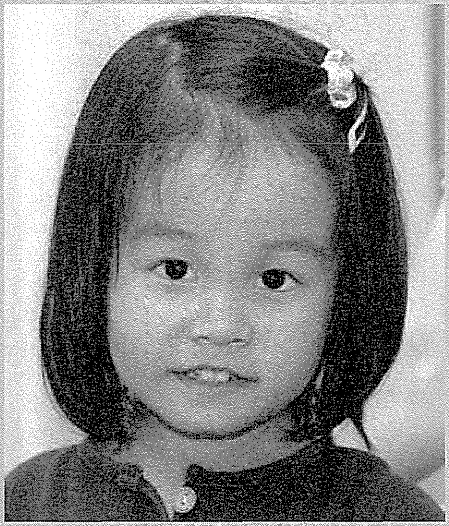

FIG. 1. Patient at the age of 5 years, showing the high forehead, broad nasal root, and thin upper lip vermilion.

Further FISH analysis for determining the breakpoint on 17p13.3 was carried out using bacterial artificial chromosome (BAC) clones that were selected from the May 2004 (NCBI35/hg17) Assembly of the UCSC Genome Browser (http://genome.ucsc.edu/) for Human. A centromere probe for chromosome 17 was used to confirm chromosome 17.

All DNAs were labeled by nick translation, according to the manufacturer's instructions (Vysis). Hybridization, post-hybridization washing, and counterstaining were performed according to standard procedures. Slides were analyzed using a completely motorized epifluorescene microscope (Leica DMRXA2) equipped with CCD camera. Both the camera and microscope were controlled with Leica CW4000 M-FISH software (Leica Microsystems Imaging Solutions, Cambridge, UK) [Yamamoto et al., 2009].

Array-CGH was performed using the Agilent SurePrint G3 Human CGH Microarray Kit 8×60K (Agilent Technologies, Inc., Santa Clara, CA) according the manufacturer's instructions. The total genomic DNA of the patient was prepared using the standard techniques. The results were analyzed using Agilent Genomic Workbench software. Only experiments having a DLR spread value <0.30 were taken into consideration.

Real-Time PCR

YWHAE is highly conserved and is ubiquitously expressed, but is expressed at highest levels in the brain [Toyo-oka et al., 2003]. To reduce the effects of SNP of *YWHAE* or other genes studied in each subject, we used lymphoblastoid cell lines [Ikeda et al., 2008].

Total RNA from lymphoblastoid cell lines were isolated with the use of a QIAamp RNA Blood Mini Kit (QIAGEN, Valencia, CA).

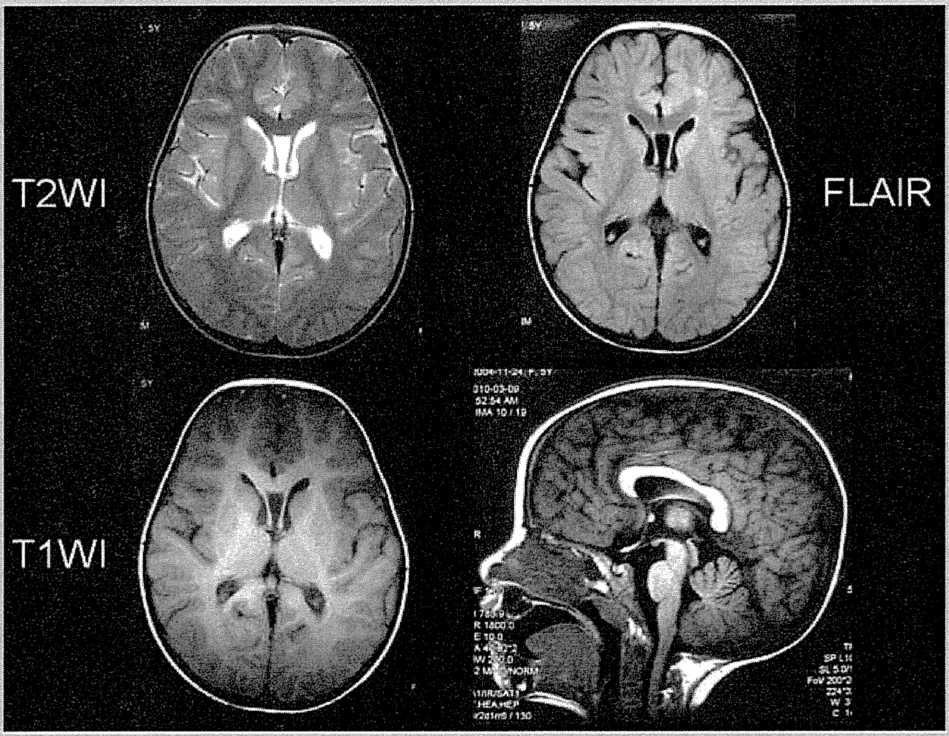

FIG. 2. Brain MRI at the age of 5 years. T1-, T2-weighted, and FLAIR images at 3-Tesla show no clinically significant abnormality but faint patchy high-intensity areas in the frontal subcortical white matter on T2-weighted and FLAIR images.

One microgram of total RNA was used for first-strand cDNA synthesis, using a Transcriptor High Fidelity cDNA synthesis kit (Roche Diagnostics, Rotkreuz, Switzerland). Real-time reverse transcription PCR was performed in a LightCycler 480 (Roche Diagnostics) using SYBR green, under the following cycling conditions: 10 min at 95°C, 45 cycles at 95°C for 30 sec, 60°C for 30 sec, and 72°C for 15 sec. The forward and reverse primer sequences used for *YWHAE* were 5′-GGATACGCTGAGTGAAGAAAGC-3′ and 5′-TATTCTGCTCTTCACCGTCACC-3′; for *PAFAH1B1*, primers were 5′-ATGGTCTCTGCTTCAGAGGATG-3′ and 5′-GTCATATCTGCAGAACAGGAAGC-3′. Beta-actin was chosen as the reference gene. Statistical analysis was performed using the delta–delta CT method. Lymphoblastoid cell lines from the patient's parents, as well as from a patient with Miller–Dieker syndrome caused by submicroscopic translocation of 17p13.3, including *PAFAH1B1* [Masuno et al., 1995], and from normal females were used for the control materials.

RESULTS

Molecular Cytogenetic and Array CGH Investigations

The complete subtelomere probe set analysis detected a 17pter deletion in the patient. However, the LIS1 probe signal was retained in the derivative chromosome. To characterize the size of the deletion, we further applied FISH analysis using the BAC clones that mapped to the region (Supplementary eFig. 1—See Supporting Information online). This revealed that the breakpoint was just on the telomeric site of the *PAFAH1B1* gene, about 2.44 Mb from 17pter (Fig. 3). The deleted region included *YWHAE* and *CRK*. Exclusion of mosaicism of the 17pter deletion was confirmed by observation on more than 100 cells.

Subsequent array CGH analysis revealed a 17p13.3 terminal microdeletion of approximately 2.3 Mb in size (chr17: −2,371, 138), which is consistent with the FISH results. No other genomic imbalances were identified on the array analysis. FISH analysis with relevant BAC clones indicated that the translocation was absent in both parents, and therefore had occurred de novo.

Real-Time PCR of YWHAE and PAFAH1B1 mRNA

We compared the expression level of *YWHAE* mRNA between the patient, her parents, a Miller–Dieker syndrome patient, and normal female controls by quantitative real-time PCR (Fig. 4). The relative expression levels were standardized to those of the patient with Miller–Dieker syndrome, which entails haploinsufficiency for both *YWHAE* and *PAFAH1B1*. We found that the *YWHAE* gene expression level in the patient was equal to that in the Miller–Dieker

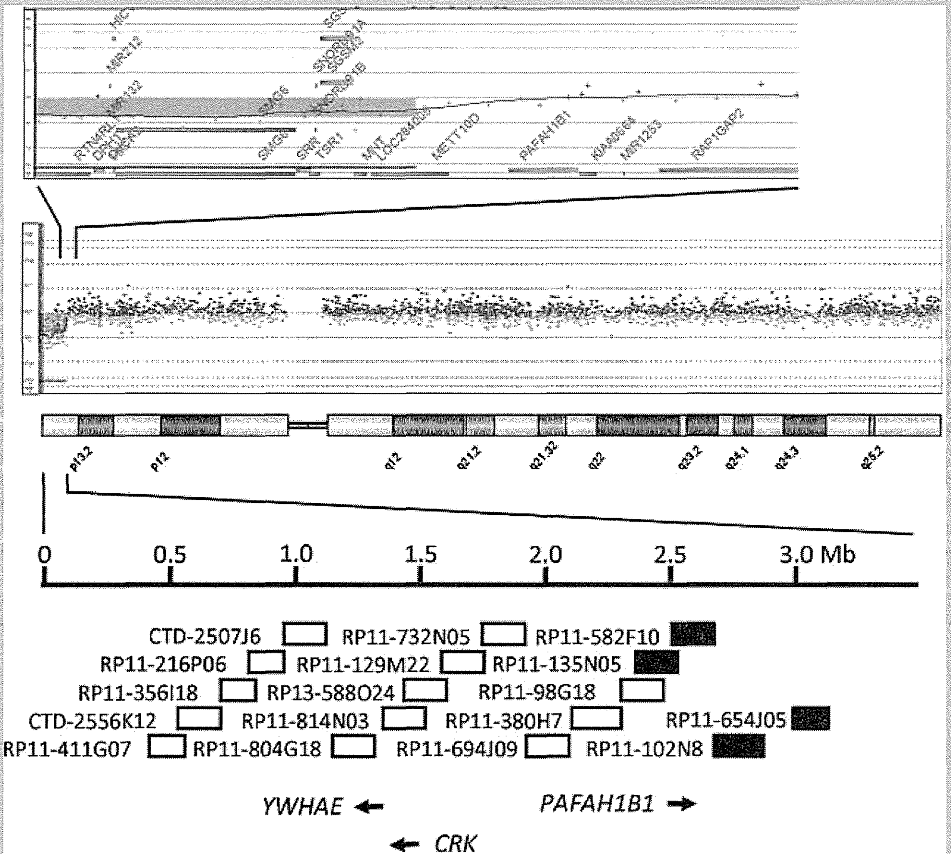
HIC
MIR212
MIR132
SMG6
SRR
TSR1
MNT
METT10D
PAFAH1B1
KIAA0664
MIR1253
RAP1GAP2
p13.2
p12
q12
q21.2
q21.32
q22
q23.2
q24.1
q24.3
q25.2
0
0.5
1.0
1.5
2.0
2.5
3.0 Mb
CTD-2507J6 ☐ RP11-732N05 ☐ RP11-582F10 ■
RP11-216P06 ☐ RP11-129M22 ☐ RP11-135N05 ■
RP11-356I18 ☐ RP13-588O24 ☐ RP11-98G18 ☐
CTD-2556K12 ☐ RP11-814N03 ☐ RP11-380H7 ☐ RP11-654J05 ■
RP11-411G07 ☐ RP11-804G18 ☐ RP11-694J09 ☐ RP11-102N8 ■
YWHAE ←
PAFAH1B1 →
← CRK

FIG. 3. Schematic representation of 17p13.3 region and bacterial artificial chromosome (BAC) clones used for refinement of the breakpoint derived from the results from array analysis. The map and position of the BAC clones are based on the information from the USCS Genome Browser (Assembly 2004, NCBI35/hg17) and Human 32K BAC Re-Array from Children's Hospital Oakland Research Institute (CHORI) BACPAC Resource. Signal retention was detected at RP11-135N5, but not at RP11-98F18, demonstrating that the breakpoint was just distal from *PAFAH1B1*. The deleted clones are indicated by open boxes, and non-deleted clones by full boxes.

syndrome patient, but was half that of her parents and normal controls. However, the expression level of *PAFAH1B1* in the patient was equal to that of the controls, but was twofold that of Miller–Dieker syndrome patient. These results were consistent with the molecular cytogenetic results.

DISCUSSION

Microdeletion of 17p13.3 involving *YWHAE*, but distal to *PAFAH1B1*, is a newly recognized syndrome associated with variable disorders of cortical development and facial dysmorphism. Here, we describe identification of a terminal microdeletion of 17p13.3 involving the *YWHAE* gene and *CRK* gene but not *PAFAH1B1*, in a girl, who had experienced mild developmental delay, short stature, and had a distinctive facial appearance, but who demonstrated normal cortical development on MRI. Expression studies of *YWHAE* and *PAFAH1B1* correlated with FISH results. This is the first report of evidence of dosage effects of the *YWHAE* gene in a patient with 17p13.3 microdeletion. *YWHAE* haploinsufficiency results in brain malformation, including cortical defects and corpus callosum hypoplasia, in both mice and humans [Toyooka et al., 2003; Mignon-Ravix et al., 2010]. However, the present case demonstrated normal brain structure on MRI. The structural brain abnormalities in patients with deletion of *YWHAE*, but not *PAFAH1B1*, have been shown to be variable; this variation included normal MRI findings [Nagamani et al., 2009; Bruno et al., 2010; Mignon-Ravix et al., 2010; Schiff et al., 2010; Shimojima et al., 2010; Tenney et al., 2011]. To our knowledge, two other cases with *YWHAE* deletion, but without obvious abnormalities on MRI, have been reported (Case DR00-063a1 in Cardoso et al. [2003], Patient 3 in Nagamani et al. [2009]). The structural variation of the brain and severity of intellectual disability or development

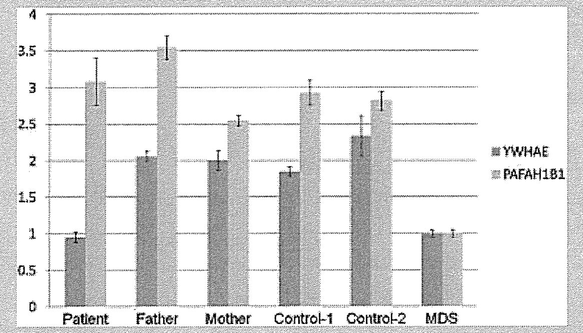

FIG. 4. Expression of *YWHAE* and *PAFAH1B1*. Quantitative measurements were standardized to the expression level in the patients with Miller–Dieker syndrome. These results were consistent with the genome copy number of each subject as indicated by FISH analysis.

represented no strict correlation in the cases with deletion of *YWHAE* but not *PAFAH1B1* (Fig. 5). These results indicated that the YWHAE plays a crucial role in neuronal development in humans, but does not result in structural abnormalities of the brain in a haploinsufficiency state. This is in contrast to *PAFAH1B1*; haploinsufficiency of this gene alone contributes to lissencephaly.

YWHAE has been shown to function within a complex with several other factors, such as PAFAH1B1 and NUDEL. Recently, using the global gene expression and pathway analysis in targeted gene mutations of *Lis1*, *Dcx*, *Ywhae*, and *Ndel1*, Pramparo et al. [2011] demonstrated that cell cycle and synaptogenesis genes are similarly expressed and are co-regulated in the developing brains of normal and mutant mouse in a time-dependent manner. Thus, reduced expression levels of *YWHAE* may still be able to mediate normal brain structure, as detected by MRI in humans [Bruno et al., 2010]. Further analysis of correlation between clinical phenotype and expression levels of related genes in brain development are required for elucidating the mechanism of neurodevelopmental disorders associated with mutations involving *YWHAE*.

The present patient we described here showed prenatal onset of growth retardation, in the absence of growth hormone deficiency; however, growth hormone therapy was effective in mediating catch-up growth from the age of 4 years. Prenatal onset of severe growth retardation is common to patients with deletions of the subtelomeric region of 17p13.3 involving *YWHAE*. However, in those cases with small, limited deletions involving *YWHAE*, growth retardation is not so as severe, as seen in Patient 1 reported by Nagamani et al. [2009] and the patient described by Mignon-Ravix et al. [2010]. Therefore, evaluation of hormones associated with growth in patients with a 17p13.3 microdeletion will also provide further insights into the genotype–phenotype correlations attributed to genes involved in these disorders.

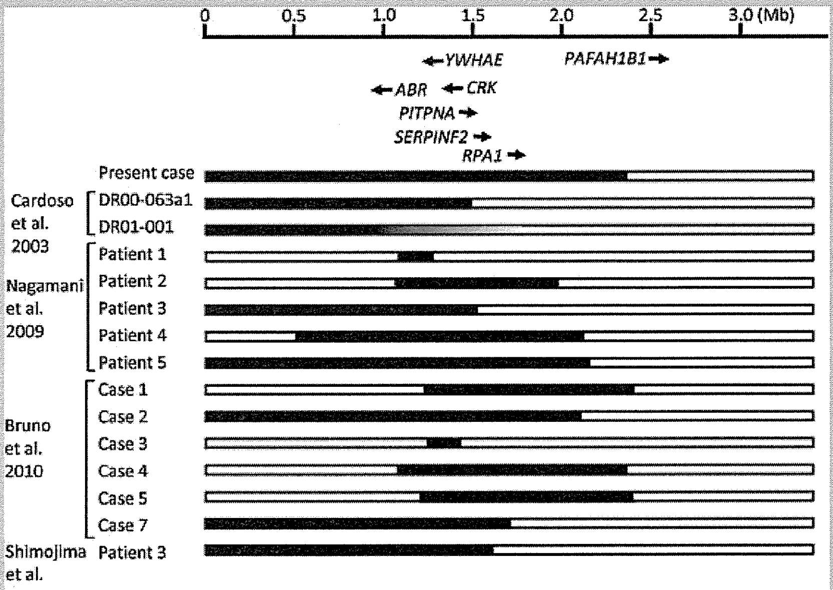

FIG. 5. Schematic representation of the microdeletion 17p13.3 including *YWHAE*, but not *PAFAH1B1*. The dark horizontal bars indicate the range of the deletion of reported patients.

ACKNOWLEDGMENTS

We thank the patient and her family for making this study possible. We are also grateful to Dr. Shuki Mizutani (Tokyo Medical and Dental University) and Dr. Hiroyuki Ida (Tokyo Jikei University) for their valuable comments. This research was supported in part by a Grant-in-aid from the Ministry of Health, Labour and Welfare, Japan.

REFERENCES

Bi W, Sapir T, Shchelochkov OA, Zhang F, Withers MA, Hunter JV, Levy T, Shinder V, Peiffer DA, Gunderson KL, Nezarati MM, Shotts VA, Amato SS, Savage SK, Harris DJ, Day-Salvatore D-L, Horner M, Lu X-Y, Sahoo T, Yanagawa Y, Beaudet AL, Cheung SW, Martinez S, Lupski JR, Reiner O. 2009. Increased LIS1 expression affects human and mouse brain development. Nat Genet 41:168–177.

Bruno DL, Anderlid BM, Lindstrand A, van Ravenswaaij-Arts C, Ganesamoorthy D, Lundin J, Martin CL, Douglas J, Nowak C, Adam MP, Kooy RF, Van der Aa N, Reyniers E, Vandeweyer G, Stolte-Dijkstra I, Dijkhuizen T, Yeung A, Delatycki M, Borgström B, Thelin L, Cardoso C, van Bon B, Pfundt R, de Vries BB, Wallin A, Amor DJ, James PA, Slater HR, Schoumans J. 2010. Further molecular and clinical delineation of co-locating 17p13.3 microdeletions and microduplications that show distinctive phenotypes. J Med Genet 47:299–311.

Cardoso C, Leventer RJ, Ward HL, Toyo-Oka K, Chung J, Gross A, Martin CL, Alanson J, Pills DT, Olney AH, Mutchinick OM, Hirotsune S, Wynshaw-Boris A, Dobyns WB, Ledbetter DH. 2003. Refinement of 400-kb critical region allows genotypic differentiation between isolated lissencepahly, Miller-Dieker syndrome, and other phenotypes secondary to deletions of 17p13.3. Am J Hum Genet 72:918–930.

Dobyns WB, Reiner O, Carrozzo R, Ledbetter DH. 1993. Lissencephaly. A human brain malformation associated with deletion of the LIS1 gene located at chromosome 17p13. JAMA 270:2838–2842(Review).

Ikeda M, Hikita T, Taya S, Uraguchi-Asaki J, Toyo-oka K, Wynshaw-Boris A, Ujike H, Inada T, Takao K, Miyakawa T, Ozaki N, Kaibuchi K, Iwata N. 2008. Identification of YWHAE, a gene encoding 14-3-3 epsilon, as a possible susceptibility gene for schizophrenia. Hum Mol Genet 17: 3212–3222.

Masuno M, Imaizumi K, Nakamura M, Matsui K, Goto A, Kuroki Y. 1995. Miller-Dieker syndrome due to maternal cryptic translocation t(10;17)-(q26.3;p13.3). Am J Med Genet 59:441–443.

Mignon-Ravix C, Cacciagli P, El-Waly B, Moncla A, Milh M, Girard N, Chabrol B, Philip N, Villard L. 2010. Deletion of YWHAE in a patient with periventricular heterotopias and pronounced corpus callosum hypoplasia. J Med Genet 47:132–136.

Nagamani SC, Zhang F, Shchelochkov OA, Bi W, Ou Z, Scaglia F, Probst FJ, Shinawi M, Eng C, Hunter JV, Sparagana S, Lagoe E, Fong CT, Pearson M, Doco-Fenzy M, Landais E, Mozelle M, Chinault AC, Patel A, Bacino CA, Sahoo T, Kang SH, Cheung SW, Lupski JR, Stankiewicz P. 2009. Microdeletions including YWHAE in the Miller-Dieker syndrome region on chromosome 17p13.3 result in facial dysmorphisms, growth restriction, and cognitive impairment. J Med Genet 46:825–833.

Pramparo T, Libiger O, Jain S, Li H, Youn YH, Hirotsune S, Schork NJ, Wynshaw-Boris A. 2011. Global developmental gene expression and pathway analysis of normal brain development and mouse models of human neuronal migration defects. PLoS Genet 7:e1001331.

Schiff M, Delahaye A, Andrieux J, Sanlaville D, Vincent-Delorme C, Aboura A, Benzacken B, Bouquillon S, Elmaleh-Berges M, Labalme A, Passemard S, Perrin L, Manouvrier-Hanu S, Edery P, Verloes A, Drunat S. 2010. Further delineation of the 17p13.3 microdeletion involving YWHAE but distal to PAFAH1B1: Four additional patients. Eur J Med Genet 53:303–308.

Shimojima K, Sugiura C, Takahashi H, Ikegami M, Takahashi Y, Ohno K, Matsuo M, Saito K, Yamamoto T. 2010. Genomic copy number variations at 17p13.3 and epileptogenesis. Epilepsy Res 89:303–309.

Tenney JR, Hopkin RJ, Schapiro MB. 2011. Deletion of 14-3-3{varepsilon} and CRK: A clinical syndrome with macrocephaly. Developmental delay, and generalized epilepsy. J Child Neurol 26:223–227.

Toyo-oka K, Shionoya A, Gambello MJ, Cardoso C, Leventer R, Ward HL, Ayala R, Tsai LH, Dobyns W, Ledbetter D, Hirotsune S, Wynshaw-Boris A. 2003. 14-3-3 Epsilon is important for neuronal migration by binding to NUDEL: A molecular explanation for Miller-Dieker syndrome. Nat Genet 34:274–285.

Yamamoto K, Yoshihashi H, Furuya N, Adachi M, Ito S, Tanaka Y, Masuno M, Chiyo H, Kurosawa K. 2009. Further delineation of 9q22 deletion syndrome associated with basal cell nevus (Gorlin) syndrome: Report of two cases and review of the literature. Congenit Anom (Kyoto) 49:8–14.

Neurogenetics (2012) 13:327–332
DOI 10.1007/s10048-012-0337-6

SHORT COMMUNICATION

A *DYNC1H1* mutation causes a dominant spinal muscular atrophy with lower extremity predominance

Yoshinori Tsurusaki · Shinji Saitoh ·
Kazuhiro Tomizawa · Akira Sudo · Naoko Asahina ·
Hideaki Shiraishi · Jun-ichi Ito · Hajime Tanaka ·
Hiroshi Doi · Hirotomo Saitsu · Noriko Miyake ·
Naomichi Matsumoto

Received: 24 February 2012 / Accepted: 3 July 2012 / Published online: 31 July 2012
© Springer-Verlag 2012

Abstract Whole-exome sequencing of two affected sibs and their mother who showed a unique quadriceps-dominant form of neurogenic muscular atrophy disclosed a heterozygous *DYNC1H1* mutation [p.H306R (c.917A>G)]. The identical mutation was recently reported in a pedigree with the axonal form of Charcot–Marie–Tooth disease. Three other missense mutations in *DYNC1H1* were also identified in families with dominant spinal muscular atrophy with lower extremity predominance. Their clinical features were consistent with those of our family. Our study has demonstrated that the same *DYNC1H1* mutation could cause spinal muscular atrophy as well as distal neuropathy, indicating pleotropic effects of the mutation.

Keywords Spinal muscular atrophy with lower extremity predominance · DYNC1H1 · Whole-exome sequencing · Charcot–Marie–Tooth disease · Allelic disease

Introduction

DYNC1H1 encodes cytoplasmic dynein heavy chain 1, which is a subunit of the primary motor protein responsible for retrograde axonal transport in neurons [1]. Weedon et al. first identified a missense mutation [p.H306R (c.917A>G)] of *DYNC1H1* in a large family with axonal Charcot–Marie–Tooth (CMT) disease by using exome sequencing, indicating the significance of *DYNC1H1* in the peripheral nerve axon [2]. Subsequently, Harms et al. reported three other missense mutations in the tail domain of *DYNC1H1* in families with dominant spinal muscular atrophy with lower extremity predominance (SMA-LED, OMIM 158600), expanding the role of *DYNC1H1* to maintenance of motor neuron itself [3]. Recently, two de novo missense mutations have also been identified in patients with severe intellectual disability and variable neuronal migration defects [4].

Authorship Y.T. and S.S. contributed equally to this work.

Y. Tsurusaki · H. Doi · H. Saitsu · N. Miyake · N. Matsumoto (✉)
Department of Human Genetics, Yokohama City University
Graduate School of Medicine,
3-9 Fukuura, Kanazawa-ku,
Yokohama 236-0004, Japan
e-mail: naomat@yokohama-cu.ac.jp

S. Saitoh (✉)
Department of Pediatrics and Neonatology, Graduate School
of Medical Sciences, Nagoya City University,
Kawasumi-1, Mizuho-cho, Mizuho-ku,
Nagoya 467-8601, Japan
e-mail: ss11@med.nagoya-cu.ac.jp

K. Tomizawa
Department of Pediatrics, Nakashibetsu Town Hospital,
Nakashibetsu, Japan

A. Sudo
Department of Pediatrics, Sapporo City General Hospital,
Sapporo, Japan

N. Asahina · H. Shiraishi
Department of Pediatrics, Hokkaido University Graduate School
of Medicine,
Sapporo, Japan

J.-i. Ito
Department of Pediatrics, Taiyo no Sono,
Date, Japan

H. Tanaka
Department of Pediatrics, Asahikawa Habilitation Center
for Disabled Children,
Asahikawa, Japan

Therefore, *DNYC1H1* may have broad biological effects on development and maintenance of the nervous system.

In this study, we describe a family containing three individuals with dominant spinal muscular atrophy with lower extremity predominance. Exome sequencing identified an identical *DYNC1H1* mutation found in a pedigree with axonal CMT [2], demonstrating the pleotropic effects of the *DYNC1H1* mutation.

Subjects and methods

Subjects

Patient 1 This female patient was born after 41 weeks of gestation. Pregnancy was uneventful. Birth weight was 3,080 g. Her initial development was normal, and head control was recognized at 3–4 months. Late infantile motor development was mildly delayed, and she could walk unassisted at 1 year and 8 months. Unstable gait persisted thereafter, and she was referred to us at 3 years and 1 month of age for evaluation. On examination, proximal lower limb-dominant muscle atrophy and decreased deep tendon reflex were noted. Gower's sign was positive. No other neurological deficits were demonstrated. No sensory disturbance or ataxia was present.

The following examinations were performed at 3 years and 1 month of age. Neither serum transaminase nor creatine kinase was elevated. Motor nerve conduction velocity was within the normal limits (55.8 m/s for the right tibial nerve). Brain MRI revealed normal findings. Muscle computed tomography (CT) demonstrated severe atrophy and lipid degeneration, predominantly in the bilateral quadriceps femoris muscle (Fig. 1). The upper limbs and distal lower limbs were not affected. A muscle biopsy from the quadriceps femoris muscle demonstrated severe grouping atrophy of type 2 fibers with a massive increase in the amount of fibrous tissue and sparse enlarged type 1 fibers (Fig. 2).

The patient is currently 18 years old and graduated from regular high school. Her motor development has steadily progressed, and she only shows moderate proximal lower limb-dominant muscle weakness and atrophy. She can walk unassisted and shows a waddling gait and positive Gower's sign. No sensory disturbance or ataxia is noted. She does not have any intellectual disability.

Patient 2 Patient 2 is the half brother of patient 1. He was born after 38 weeks of gestation to the same mother and a different father from patient 1's. His birth weight was 2,405 g. He could control his head at 3–4 months, turn over at 6 months, and sit unassisted at 7–8 months. His motor development was delayed thereafter, and he walked unassisted at 1 year and 7 months. His mental development was normal. Because of a persistently unstable gait, he was hospitalized and examined at 5 years and 11 months. Physical examination revealed moderate muscle weakness in the proximal lower limb, but Gower's sign was negative. Deep tendon reflex was normal. No sensory disturbance or ataxia was recognized. Ankle joint contracture and foot deformity were absent.

The following examinations were performed at 5 years and 11 months of age. Serum transaminase and creatine kinase levels were normal. Brain and spinal MRI revealed no abnormal findings. Motor nerve conduction velocity and amplitude were within the normal limits (51.1 m/s, 4.6 mV for the right median nerve, 51.1 m/s, 9.9 mV for the right tibial nerve). Sensory nerve conduction velocity and amplitude were also within the normal limits (57.3 m/s, 28.4 uV for the right median nerve, 63.7 m/s, 9.6 uV for the right sural nerve). Needle electromyography of the anterior tibial muscle showed long high-amplitude discharges (3.5–4.0 mV, 10 ms) consistent with a neurogenic pattern, although no denervation potential, including positive sharp wave or fibrillation potential, was present, while the right biceps brachii showed inconclusive results. Muscle CT revealed severe atrophy and lipid degeneration, most predominantly in the bilateral quadriceps femoris. The upper limbs and distal lower limbs were not affected (Fig. 1).

The patient is now 12 years old and can walk unassisted but with a waddling gait. He has shown no further deterioration of motor function. Proximal lower limb weakness and wasting are evident, but the patient shows no upper limb weakness. No sensory disturbance or ataxia has been recognized.

Patient 3 Patient 3 is the mother of the two sibs. She is currently 50 years of age. No family history (except for her children) of neuromuscular disorders was noted. Until we examined the second sib, she had not been noted to have proximal lower limb muscle weakness. She did not recall her infantile development, and it was impossible to obtain further information. She graduated from a regular high school, married, and raised her children. She has not shown any neurological deterioration. She did not show a waddling gait, but had difficulty squatting. She was examined at 44 years of age. Her deep tendon reflex was normal, and no ankle joint contracture was present. Muscle CT revealed bilateral quadriceps-dominant muscle atrophy and lipid degeneration (Fig. 1). She also demonstrated mild muscle atrophy in her hip. Unfortunately, CT of the distal lower limb muscle could not be performed.

Exome sequencing

We performed the whole-exome sequencing of two patients (II-1 and II-2; Fig. 3a). Three micrograms of genomic DNA

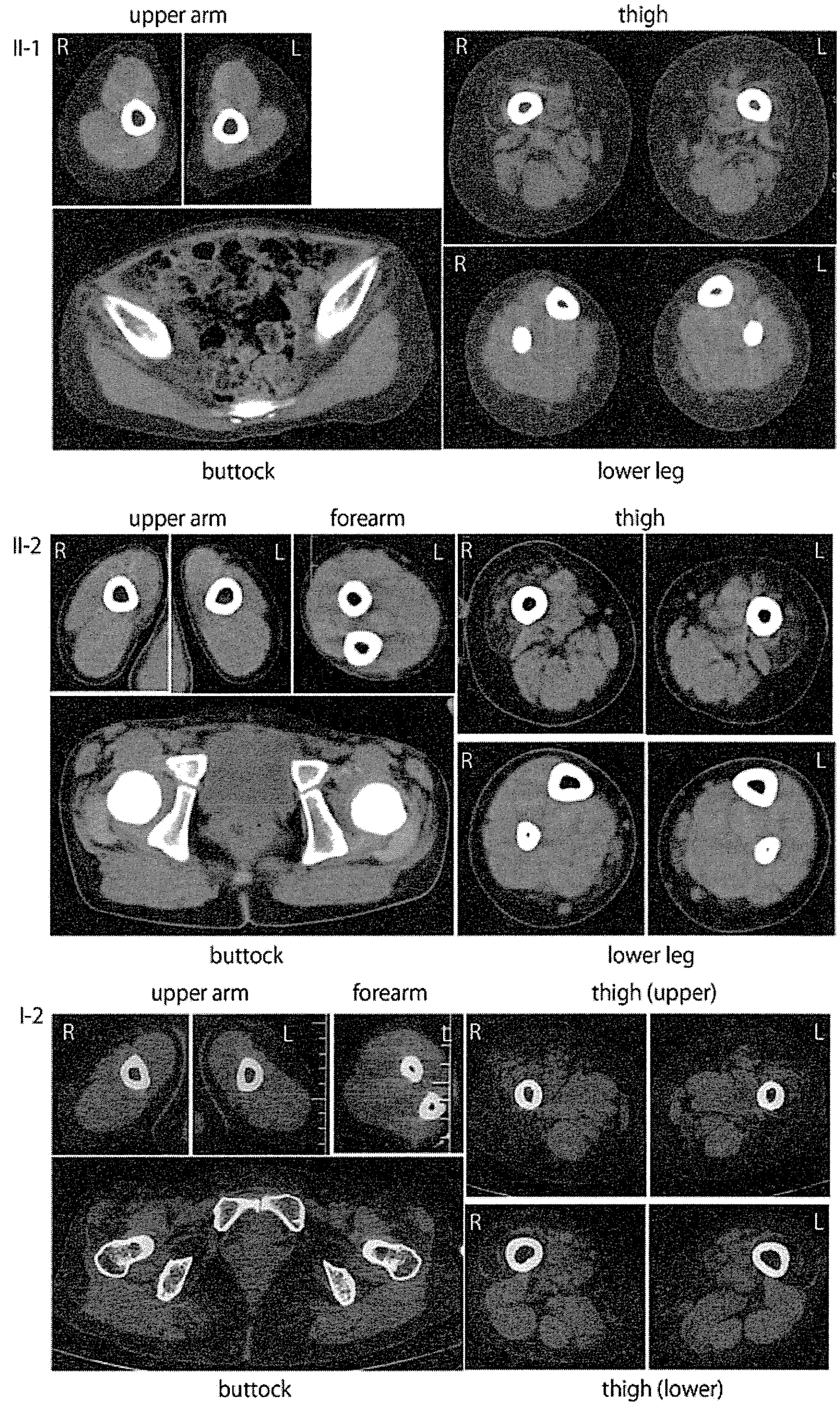
upper arm
thigh
II-1
R
L
R
L
R
L
buttock
lower leg
upper arm
forearm
thigh
II-2
R
L
L
R
L
R
L
buttock
lower leg
upper arm
forearm
thigh (upper)
I-2
R
L
L
R
L
R
L
buttock
thigh (lower)

Fig. 1 Muscle imaging. Muscle computed tomography images of patient II-1 at the age of 3 years and 1 month (*upper*), patient II-2 at the age of 5 years and 11 months (*middle*), and patient I-1 at the age of 44 years (*lower*) are displayed. *R* right, *L* left

was processed using a SureSelect Human All Exon Kit v.1 (approximately 180,000 exons covering 38 Mb of the CCDS database) (Agilent Technologies, Santa Clara, CA) according to the manufacturer's protocol. Captured DNA was diluted to a concentration of 8 pM and sequenced on a Genome Analyzer IIx (Illumina, San Diego, CA) with 76-bp paired-end reads. We used two of the eight lanes in the flow cell (Illumina). Image analyses and base calling were performed by sequence control software real-time analysis and/or Off-line Basecaller software v1.6.0 (Illumina). Alignment was performed using CASAVA software v1.6.0. The quality-controlled (Path Filter) reads were mapped to the human reference genome (UCSC hg19, NCBI build 37), using mapping and assembly with quality (MAQ) and NextGENe software v2.0 (SoftGenetics, State College, PA). SNPs in MAQ-passed reads were annotated using the

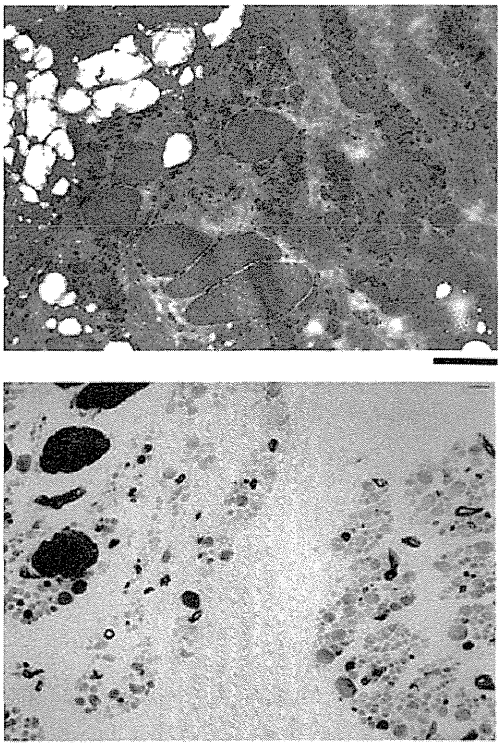

Fig. 2 Histological study. Hematoxylin–eosin staining (*upper*) and ATPase staining (pH=4.6, *lower*) of the quadriceps femoris muscle of patient II-1. The *scale bar* indicates 100 μm in length

SeattleSeq Annotation website (http://gvs.gs.washington.edu/SeattleSeqAnnotation/).

Priority scheme and capillary sequencing

We adopted a prioritization scheme used in recent studies to identify the pathogenic mutation [5–7]. Called variants found by each informatics method filtered into unregistered variants (excluding registered dbSNP131 and 1,000 genomes), overlapping variants called in common by NextGENe and MAQ, nonsynonymous changes (NS), splice site mutations (±2 bp from the exon–intron junctions) (SS), small insertions or deletions (indels), and overlapping variants called in II-1 and II-2 were checked, and variants found in our 33 in-house exomes derived from 19 healthy individuals and 14 individuals with unrelated diseases were excluded (Table 1). An online human genome mutation database (HGMD, https://portal.biobase-international.com/hgmd/pro/start.php) was referred to as a reference for disease-causing mutations. The variants were confirmed as true positives by Sanger sequencing of polymerase chain reaction products amplified using genomic DNA as a template. Sanger sequencing was performed on an ABI3500XL or ABI3100 autosequencer (Life Technologies, Carlsbad, CA). Sequencing data were analyzed using Sequencer software (Gene Codes Corporation, Ann Arbor, MI).

A total of 177 Japanese control samples (354 alleles) were check by high-resolution melting analysis using a LightCycler 480 (Roche Diagnostics, Otsu, Japan) to see the variant frequency. The reaction was performed in 10 μl containing 10 ng of genomic DNA, 0.2 mM dNTPs,

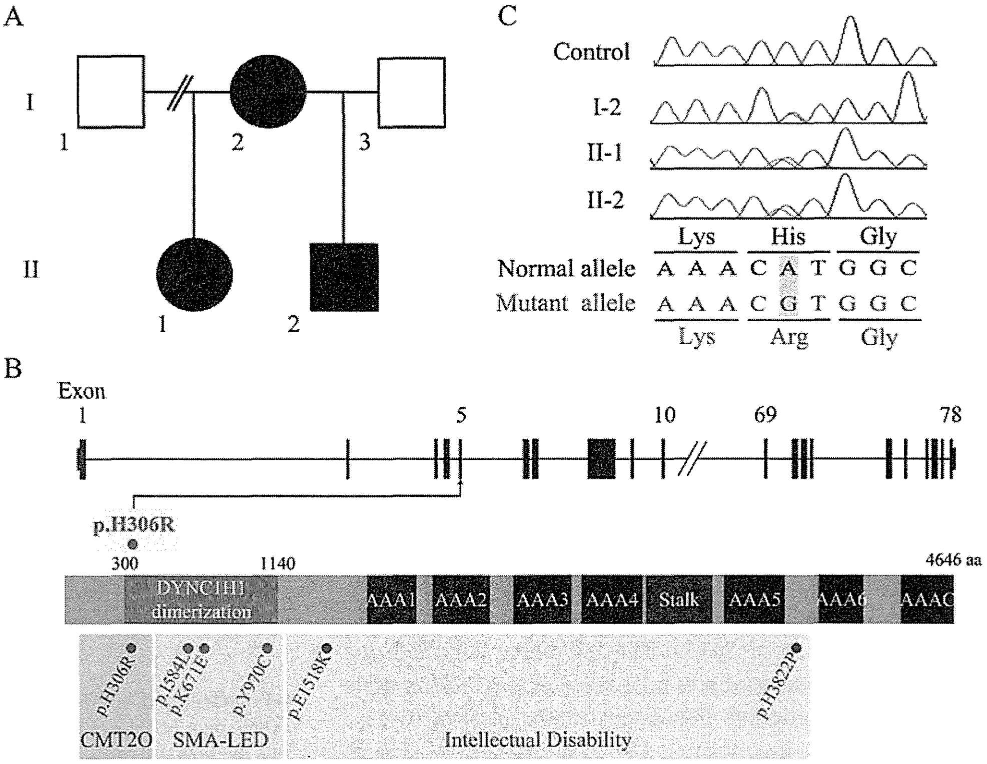
A
I
1
2
3
II
1
2
C
Control
I-2
II-1
II-2
Lys His Gly
Normal allele A A A C A T G G C
Mutant allele A A A C G T G G C
Lys Arg Gly
B
Exon
1
5
10
69
78
p.H306R
300
1140
4646 aa
DYNC1H1 dimerization
AAA1
AAA2
AAA3
AAA4
Stalk
AAA5
AAA6
AAAC
p.H306R
p.I584L
p.K671E
p.Y970C
p.E1518K
p.H3822P
CMT2O
SMA-LED
Intellectual Disability

Fig. 3 Genetic study. **a** Familial pedigree. **b** The gene structure of *DYNC1H1* with the mutation [p.H306R (c.917A>G)] (*upper*), the protein structure with functional domains (*middle*), and reported mutations corresponding to respective diseases (*lower*). *AAA* ATPase domains (AAA 1 to 6), *AAAC* unrelated seventh domain. **c** Sequences of a control and the family members are displayed. Heterozygous mutations are observed in patients I-2, II-1, and II-2

Table 1 Variant priority scheme of exome sequencing data

	Half sister		Half brother	
	NextGENe	MAQ (SeattleSeq)	NextGENe	MAQ (SeattleSeq)
Total variants called	73,966	174,757	73,370	163,707
Autosomal+chr X	71,522	174,165	70,068	163,013
Unknown SNP variants (dbSNP, 1,000 genomes)	11,132	21,284	10,857	19,858
Overlap of NextGENe and MAQ	1,598		1,482	
NS/SS/I	426		411	
Overlapping in half sibs	135			
Unknown variants (in-house database)	62			

MAQs were annotated using SeattleSeq annotation. The annotation includes gene names, dbSNP rs IDs, and SNP functions (e.g., missense), protein positions and amino acid changes. *NS* nonsynonymous, *SS* splice site (±2 bp), *I* indels

0.125 U of ExTaq (Takara Bio, Inc., Otsu, Japan), 1× buffer, and 1.5 μM SYTO9 (Invitrogen, Carlsbad, CA).

Results

Approximately 9.8 and 9.5 Gb of sequence data were generated for II-1 and II-2, respectively. This approach resulted in more than 85.8 % (II-1) and 86.5 % (II-2) of the target regions being covered by ten reads or more. Two informatics methods identified 62 potentially pathogenic changes (Table 1). We found a missense mutation [p.H306R (c.917A>G)] in *DYNC1H1* from among 62 variants using the HGMD as a reference; this mutation has been reported as a causative mutation for CMT disease [2]. The heterozygous missense mutation was confirmed in I-2, II-1, and II-2 (Fig. 3b). This missense mutation was not found in 177 control samples.

Discussion

The identical *DYNC1H1* mutation (p.H306R) found in a large pedigree with axonal type of CMT disease was detected by exome sequencing in a family with a unique form of quadriceps-dominant neurogenic muscular atrophy [2]. Three members of the family demonstrated very similar clinical features, which were distinct from CMT disease. The most striking feature was a unique distribution of muscle involvement. The quadriceps femoris muscle was almost selectively involved in the early course of the disease, and the proximal lower limb was predominantly involved throughout the disease course. Recently, three other missense mutations were detected in families with SMA-LED. Clinical features of the current family are essentially consistent with those of SMA-LED, hallmarks of which are early childhood onset of proximal leg weakness with muscle atrophy and nonlength-dependent motor neuron disease without sensory involvement [3]. Nonprogressive clinical course despite early childhood onset as in our family should be another hallmark of SMA-LED. These cumulative data clearly indicate that *DYNC1H1* plays an essential role in maintenance of spinal motor neurons and their axon.

Thus far, four missense mutations (p.H306R, p.I584L, p.K671E, p.Y970C) identified in human cases of CMT or SMA-LED are located in the same tail domain for DYNC1H1 dimerization. It is of note that three missense mutations (p.F580Y, p.G1042A, p.T1057C) found in mouse models are also located in the tail domain [8–10]. These mice involve not only spinal motor neurons but also sensory and cortical neurons. The tail domain is thought to be essential for dimerization of dynein heavy chains, and thus, missense mutations in the tail domain may disrupt function of dynein complex formation in a dominant negative manner. Two distinct de novo mutations (p.E1518K, p.H3822P) identified in patients with severe intellectual disability and variable neuronal migration defects were located outside of the tail domain. These patients also showed possible peripheral nerve involvement, but formal neurophysiological investigation was not available. Since mice with *Dync1h1* abnormality show broad central nervous system involvement, *DNYC1H1* is likely to cause a wide range of neuronal migration disorders.

CMT disease with the p.H306R mutation has been designated as CMT2O (OMIM 614228). Most members of the pedigree with p.H306R reported by Weedon et al. demonstrated distal dominant muscle weakness, while one patient showed proximal lower limb-dominant muscle atrophy as in our family [2]. Therefore, the same missense mutation in the tail domain could cause CMT2O phenotype and SMA-LED phenotype even within the same pedigree. It is hard to explain the underlying mechanism of pleotropic effects of the mutation. Further studies are absolutely necessary to elucidate phenotype–genotype correlation and pleiotropic mutational consequences.

Acknowledgments We would like to thank the family for their participation in this study. This work was supported by research grants from the Ministry of Health, Labour and Welfare (H.S., N. Miyake, and

N. Matsumoto); a Grant-in-Aid for Scientific Research from the Japan Society for the Promotion of Science (N. Miyake and N. Matsumoto); a grant from the Japan Science and Technology Agency (N. Matsumoto), the Strategic Research Program for Brain Sciences (N. Matsumoto); a Grant-in-Aid for Scientific Research on Innovative Areas (Foundation of Synapse and Neurocircuit Pathology) from the Ministry of Education, Culture, Sports, Science and Technology of Japan (N. Matsumoto); a research grant from Naito Foundation (N. Matsumoto); and research grants from Takeda Science Foundation (N. Miyake and N. Matsumoto). This work was performed at the Advanced Medical Research Center, Yokohama City University, Japan.

References

1. Pfister KK, Shah PR, Hummerich H, Russ A, Cotton J, Annuar AA, King SM, Fisher EM (2006) Genetic analysis of the cytoplasmic dynein subunit families. PLoS Genet 2(1):e1. doi:10.1371/journal.pgen.0020001
2. Weedon MN, Hastings R, Caswell R, Xie W, Paszkiewicz K, Antoniadi T, Williams M, King C, Greenhalgh L, Newbury-Ecob R, Ellard S (2011) Exome sequencing identifies a DYNC1H1 mutation in a large pedigree with dominant axonal Charcot–Marie–Tooth disease. Am J Hum Genet 89(2):308–312. doi:10.1016/j.ajhg.2011.07.002
3. Harms MB, Ori-McKenney KM, Scoto M, Tuck EP, Bell S, Ma D, Masi S, Allred P, Al-Lozi M, Reilly MM, Miller LJ, Jani-Acsadi A, Pestronk A, Shy ME, Muntoni F, Vallee RB, Baloh RH (2012) Mutations in the tail domain of DYNC1H1 cause dominant spinal muscular atrophy. Neurology 78(22):1714–1720. doi:10.1212/WNL.0b013e3182556c05
4. Willemsen MH, Vissers LE, Willemsen MA, van Bon BW, Kroes T, de Ligt J, de Vries BB, Schoots J, Lugtenberg D, Hamel BC, van Bokhoven H, Brunner HG, Veltman JA, Kleefstra T (2012) Mutations in DYNC1H1 cause severe intellectual disability with neuronal migration defects. J Med Genet 49(3):179–183. doi:10.1136/jmedgenet-2011-100542
5. Tsurusaki Y, Okamoto N, Suzuki Y, Doi H, Saitsu H, Miyake N, Matsumoto N (2011) Exome sequencing of two patients in a family with atypical X-linked leukodystrophy. Clin Genet 80(2):161–166. doi:10.1111/j.1399-0004.2011.01721.x
6. Saitsu H, Osaka H, Sasaki M, Takanashi J, Hamada K, Yamashita A, Shibayama H, Shiina M, Kondo Y, Nishiyama K, Tsurusaki Y, Miyake N, Doi H, Ogata K, Inoue K, Matsumoto N (2011) Mutations in POLR3A and POLR3B encoding RNA polymerase III subunits cause an autosomal-recessive hypomyelinating leukoencephalopathy. Am J Hum Genet 89(5):644–651. doi:10.1016/j.ajhg.2011.10.003
7. Doi H, Yoshida K, Yasuda T, Fukuda M, Fukuda Y, Morita H, Ikeda S, Kato R, Tsurusaki Y, Miyake N, Saitsu H, Sakai H, Miyatake S, Shiina M, Nukina N, Koyano S, Tsuji S, Kuroiwa Y, Matsumoto N (2011) Exome sequencing reveals a homozygous SYT14 mutation in adult-onset, autosomal-recessive spinocerebellar ataxia with psychomotor retardation. Am J Hum Genet 89(2):320–327. doi:10.1016/j.ajhg.2011.07.012
8. Hafezparast M, Klocke R, Ruhrberg C, Marquardt A, Ahmad-Annuar A, Bowen S, Lalli G, Witherden AS, Hummerich H, Nicholson S, Morgan PJ, Oozageer R, Priestley JV, Averill S, King VR, Ball S, Peters J, Toda T, Yamamoto A, Hiraoka Y, Augustin M, Korthaus D, Wattler S, Wabnitz P, Dickneite C, Lampel S, Boehme F, Peraus G, Popp A, Rudelius M, Schlegel J, Fuchs H, Hrabe de Angelis M, Schiavo G, Shima DT, Russ AP, Stumm G, Martin JE, Fisher EM (2003) Mutations in dynein link motor neuron degeneration to defects in retrograde transport. Science 300(5620):808–812. doi:10.1126/science.1083129
9. Chen XJ, Levedakou EN, Millen KJ, Wollmann RL, Soliven B, Popko B (2007) Proprioceptive sensory neuropathy in mice with a mutation in the cytoplasmic dynein heavy chain 1 gene. J Neurosci 27(52):14515–14524. doi:10.1523/JNEUROSCI.4338-07.2007
10. Ori-McKenney KM, Vallee RB (2011) Neuronal migration defects in the Loa dynein mutant mouse. Neural Dev 6:26. doi:10.1186/1749-8104-6-26

RESEARCH ARTICLE

AMERICAN JOURNAL OF
medical genetics
PART A

MBTPS2 Mutation Causes BRESEK/BRESHECK Syndrome

Misako Naiki,[1,2] Seiji Mizuno,[3] Kenichiro Yamada,[1] Yasukazu Yamada,[1] Reiko Kimura,[1] Makoto Oshiro,[4] Nobuhiko Okamoto,[5] Yoshio Makita,[6] Mariko Seishima,[7] and Nobuaki Wakamatsu[1]*

[1]Department of Genetics, Institute for Developmental Research, Aichi Human Service Center, Kasugai, Aichi, Japan

[2]Department of Pediatrics, Nagoya University Graduate School of Medicine, Nagoya, Aichi, Japan

[3]Department of Pediatrics, Central Hospital, Aichi Human Service Center, Kasugai, Aichi, Japan

[4]Department of Pediatrics, Japanese Red Cross Nagoya Daiichi Hospital, Nagoya, Aichi, Japan

[5]Department of Medical Genetics, Osaka Medical Center and Research Institute for Maternal and Child Health, Izumi, Osaka, Japan

[6]Education Center, Asahikawa Medical University, Asahikawa, Hokkaido, Japan

[7]Department of Dermatology, Gifu University Graduate School of Medicine, Gifu, Gifu, Japan

Received 25 July 2011; Accepted 17 October 2011

BRESEK/BRESHECK syndrome is a multiple congenital malformation characterized by brain anomalies, intellectual disability, ectodermal dysplasia, skeletal deformities, ear or eye anomalies, and renal anomalies or small kidneys, with or without Hirschsprung disease and cleft palate or cryptorchidism. This syndrome has only been reported in three male patients. Here, we report on the fourth male patient presenting with brain anomaly, intellectual disability, growth retardation, ectodermal dysplasia, vertebral (skeletal) anomaly, Hirschsprung disease, low-set and large ears, cryptorchidism, and small kidneys. These manifestations fulfill the clinical diagnostic criteria of BRESHECK syndrome. Since all patients with BRESEK/BRESHECK syndrome are male, and X-linked syndrome of ichthyosis follicularis with atrichia and photophobia is sometimes associated with several features of BRESEK/BRESHECK syndrome such as intellectual disability, vertebral and renal anomalies, and Hirschsprung disease, we analyzed the causal gene of ichthyosis follicularis with atrichia and photophobia syndrome, *MBTPS2*, in the present patient and identified an p.Arg429His mutation. This mutation has been reported to cause the most severe type of ichthyosis follicularis with atrichia and photophobia syndrome, including neonatal and infantile death. These results demonstrate that the p.Arg429His mutation in *MBTPS2* causes BRESEK/BRESHECK syndrome. © 2011 Wiley Periodicals, Inc.

Key words: BRESEK/BRESHECK syndrome; IFAP syndrome; *MBTPS2*; mutation; S2P

How to Cite this Article:
Naiki M, Mizuno S, Yamada K, Yamada Y, Kimura R, Oshiro M, Okamoto N, Makita Y, Seishima M, Wakamatsu N. 2011. *MBTPS2* mutation causes BRESEK/BRESHECK syndrome.
Am J Med Genet Part A .

INTRODUCTION

BRESEK/BRESHECK syndrome (OMIM# 300404), a multiple congenital malformation disorder characterized by brain anomalies, intellectual disability, ectodermal dysplasia, skeletal deformities, Hirschsprung disease, ear or eye anomalies, cleft palate or cryptorchidism, and kidney dysplasia/hypoplasia [Reish et al., 1997]. The acronym BRESEK refers to the common findings, whereas BRESHECK refers to all manifestations. Because the first two patients were maternally related half brothers, an X-linked disorder was proposed. Although each symptom of these patients is often observed in other congenital diseases, the combination of all symptoms is rare, and only one additional patient with BRESEK has been reported to date [Tumialán and Mapstone, 2006]. Here, we present the fourth male patient with multiple anomalies. The patient presented with a variety of clinical features that were consistent with those of the previously reported BRESHECK syndrome.

The syndrome of ichthyosis follicularis with atrichia and photophobia (IFAP, OMIM# 308205), an X-linked recessive oculocutaneous disorder, is characterized by a peculiar triad of ichthyosis follicularis, total or subtotal atrichia, and varying degrees

---

Grant sponsor: Takeda Science Foundation; Grant sponsor: Health Labour Sciences Research Grant.

*Correspondence to:
Nobuaki Wakamatsu, Department of Genetics, Institute for Developmental Research, Aichi Human Service Center, 713-8 Kamiya-cho, Kasugai, Aichi 480-0392, Japan. E-mail: nwaka@inst-hsc.jp

Published online 00 Month 2011 in Wiley Online Library (wileyonlinelibrary.com).

DOI 10.1002/ajmg.a.34373

© 2011 Wiley Periodicals, Inc.

of photophobia [MacLeod, 1909]. Martino et al. [1992] reported a male patient with IFAP syndrome presented with short stature, intellectual disability, seizures, hypohidrosis, enamel dysplasia, congenital aganglionic megacolon, inguinal hernia, vertebral and renal anomalies, and the classic symptom triad of IFAP syndrome. This report broadened the clinical features of IFAP syndrome. It should be noted that the clinical symptoms of this patient are quite similar to those of BRESHECK syndrome, with the exception of cleft palate, cryptorchidism, and photophobia (Patient 5; Table I). The gene mutated in patients with IFAP syndrome, *MBTPS2* (GenBank reference sequence NM_015884), was identified from a variety of clinical features of IFAP syndrome, including the triad and neonatal death [Oeffner et al., 2009]. Thus, the mode of inheritance and several clinical features are common to both BRESEK/BRESHECK and IFAP syndromes. These findings prompted us to perform mutation analysis of *MBTPS2* in the present patient, resulting in the identification of a missense mutation.

MATERIALS AND METHODS

Patients

Written informed consent was obtained from the parents of the patient. Experiments were conducted after approval of the institutional review board of the Institute for Developmental Research, Aichi Human Service Center. The patient (II-1; Fig. 3) was born to a 31-year-old mother (I-2) and a 31-year-old father (I-1), both healthy Japanese individuals without consanguinity. His mother miscarried her first child at 5 weeks. The pregnancy of the patient reported here was complicated with mild oligohydramnios, and he was delivered by caesarean because of a breech position at 38 weeks of gestation. His birth weight was 1,996 g (−2.6 SD), and he measured 44 cm (−2.6 SD) in length with an occipitofrontal circumference of 32.5 cm (−0.5 SD). Apgar scores at 1 and 5 min were four and eight, respectively. The patient exhibited generalized alopecia and lacked eyelashes, scalp hair, and eyebrows (Fig. 1A). The skin on the entire body was erythematous with

TABLE I. Clinical Features of BRESEK/BRESHECK and IFAP Syndromes and *MBTPS2* Mutation

	BRESEK/BRESHECK syndrome				IFAP syndrome		
Patient	**1**	**2**	**3**	**4**	**5**	**6**	**7**
Clinical features							
Gender	M	M	M	M	M	M	M
Gestational age (weeks)	32	40	ND	38	30	ND	ND
Birth weight (g)	990	2,230	ND	1,996	2,040	ND	ND
Intrauterine growth retardation	+	+	ND	+	−	ND	ND
Major features							
Follicular ichthyosis	−	−	ND	−	+	+	+
Atrichia	+	+	+	+	+	+	+
Photophobia	−	−	−	+	+	+	+
Brain malformation	+	+	+	+	+	−	+
Mental and growth retardation	+	+	+	+	+	+	+
Skeletal (Vertebrate) anomalies	+	+	+	+	+	+	+
Hirschsprung disease	−	+	+	+	+	+	+
Eye malformation or	+	+	+	−	+	−	−
Large ears	+	+	+	+	+	−	−
Cleft lip/palate or	−	+	−	−	−	+	−
Cryptorchidism	+	+	−	+	−	−	−
Kidney malformation	+	+	−	+	+	+	+
Other features							
Microcephaly	+	+	+	+	+	−	+
Seizures	−	+	+	+	+	−	+
Deafness	−	+	−	+	−	−	−
Hand anomalies	+	+	+	−	+	+	+
Cardiac anomalies	−	−	+	−	−	−	+
Inguinal hernia	−	−	−	−	+	+	+
Trachea anomalies	−	−	−	+	−	−	−
Regression	−	−	−	+	−	−	−
Age	6 h d	7 y	1.5 y	8 y	3 y	9 m d	14 m d
MBTPS2 mutation	NP	NP	NP	R429H	NP	R429H	R429H

+, present;−, not present; M, male; ND, not described; NP, not performed; h, hour; d, dead; m, month; y, year; R429H, Arg429His; BRESEK/BRESHECK syndrome, (Patients 1-4); IFAP syndrome, (Patients 5–7); Patients: 1, Reish et al. [1997] patient 1; 2, Reish et al. [1997] patient 2; 3, Tumialán and Mapstone [2006]; 4, present case; 5, Martino et al. [1992]; 6, Oeffner et al. [2009] 3-III:3; 7, Oeffner et al. [2009] 3-III:4.

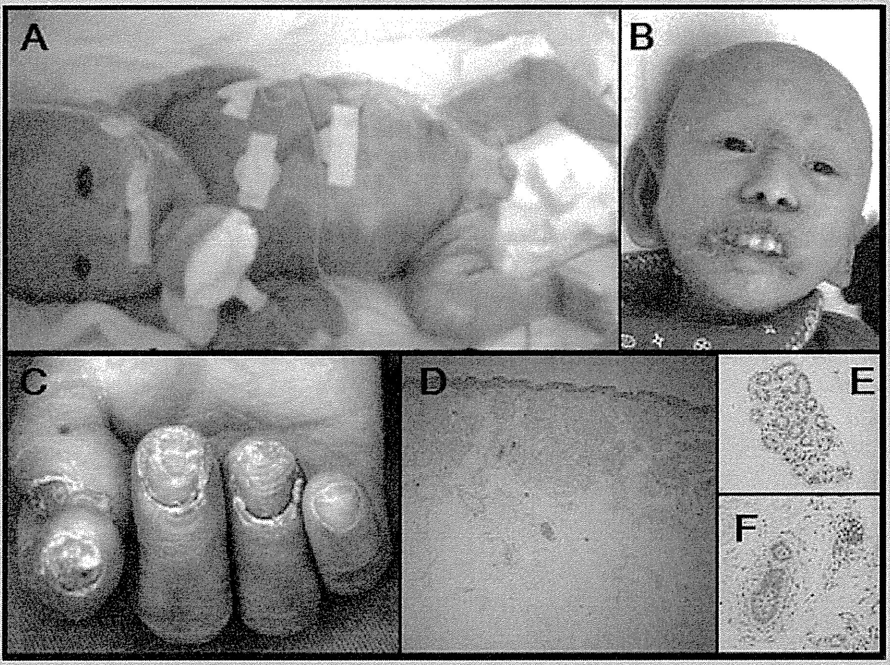

FIG. 1. Clinical appearance and dermatological findings of the patient. A: Lateral view of the patient at birth. Note the generalized alopecia with an absence of scalp hair, eyebrows, and eyelashes. The skin was dry and scaly, and an itchy erythema was observed over the entire body. B: Frontal view of the patient at 4 years of age. Note the characteristic facial appearance with long, malformed ears, a relatively high nasal bridge, and a wide nasal base. C: The patient had normal-sized but deformed and thickened nails. D–F: Histologic examination of the abdominal skin at the age of 15 months showed a reduced number of hair follicles (D), normal eccrine glands (E), and hypoplastic hair follicles (F).

continuous desquamation (Fig. 1A). He had malformed large ears, an inferiorly curved penis, and a bifid scrotum. The testicles were not palpable. He experienced persistent constipation, and total colonic Hirschsprung disease was confirmed through barium enema (Fig. 2E) and rectal biopsy at 2 months. A bone survey performed using three-dimensional (3D) computed tomography (CT) showed abnormal imbalanced hemivertebrae in the two lowest thoracic vertebral bodies (Fig. 2C). The patient's right kidney was smaller than normal. Brain magnetic resonance imaging (MRI) at 3 years of age demonstrated decreased volumes of the frontal and parietal lobes and thinning of the corpus callosum with dilatation of the ventricles (Fig. 2A,B). There were no abnormalities of the eyes or optic nerves. We concluded that the patient had BRESHECK syndrome. The patient had seizures at 5 months of age with an apneic episode and cyanosis. Electroencephalographic (EEG) analysis showed abnormal patterns of sharp waves in the posterior lobe. The seizures were almost completely controlled with phenobarbital. The patient was allergic to milk. At 7 months, tracheal endoscopy revealed subglottic tracheal stenosis and abnormal segmentation of the left lung. A chest CT performed at 3 years of age showed a congenital cystic adenomatoid malformation (CCAM) in the right upper lobe (Fig. 2D). Auditory brain stem responses showed bilateral 80 dB hearing loss at 8 months of age.

The patient exhibited delayed psychomotor development during his infancy. He could drink from a bottle at the age of 3 months and could sit up unsupported at 15 months. Abdominal skin biopsy at 15 months revealed reduced number of hair follicles (Fig. 1D). The eccrine glands were normal (Fig. 1E), and most of his hair follicles appeared to be hypoplastic (Fig. 1F). These findings were similar to ichthyosiform erythroderma. Photophobia was noted when the patient left the hospital and first went outside at 18 months of age. At 2 years and 6 months of age, he had a series of epileptic episodes. He experienced a maximum of 100 seizures per day, and EEG analysis showed continual abnormal spikes in the posterior lobe. The seizures were controlled with clonazepam therapy. At 2 years and 9 months of age, he could stand with support and displayed social smiles when interacting with other people. However, the patient developed psychomotor regression at the age of 3 years. He exhibited a progressive loss of emotional response to others, developed hypotonia, and could not stand or sit alone. At 4 years of age, he became bedridden and showed almost no response to people. He had highly desquamated skin, similar to that seen in ichthyosis (Fig. 1B), and easily developed erythema on the skin of the entire body. The patient had deformed and thickened nails (Fig. 1C). He had persistent corneal erosions, but ophthalmoscopy could not be performed at the age of 4 years because of corneal opacification.

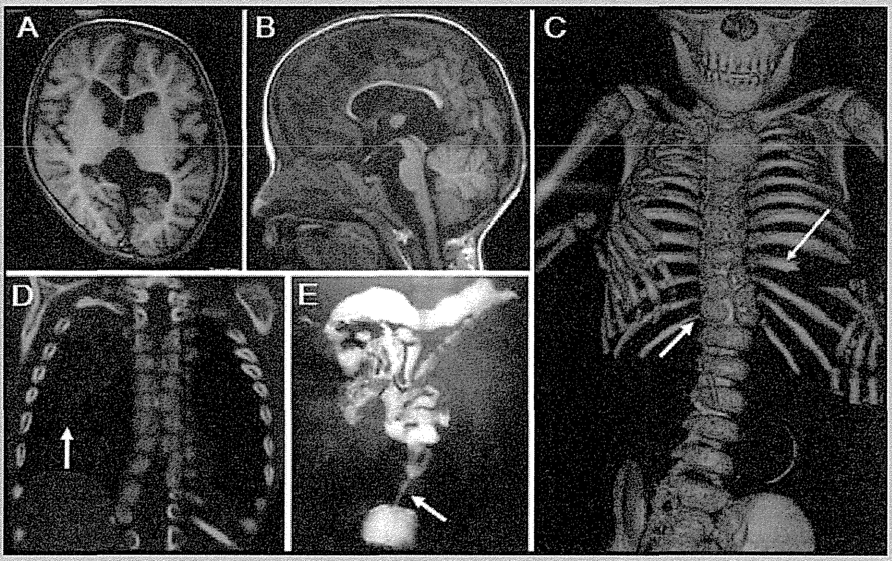

FIG. 2. CT and MRI findings of the patient. A,B: Brain MRI (T1-weighted image) at 3 years of age showed decreased volume of the cortex in the frontal and parietal lobes, the presence of a subdural cyst in the corpora quadrigemina, and dilatation of the lateral and fourth ventricle. C: A bone survey performed using 3D CT showed abnormal segmentation of the ninth rib and an imbalanced hemivertebrae in the two lowest thoracic vertebral bodies (shown with arrows). D: CT of the chest showed CCAM (indicated by the arrow) in the right upper lobe. E: Barium enema showed a reduced caliber rectum (indicated by the arrow), suggesting that the patient had Hirschsprung disease.

Chromosomal and Molecular Genetic Studies

Genomic DNA isolated from the patient's peripheral white cells by phenol/chloroform extraction was used for *MBTPS2* mutation analysis. PCR-amplified DNA fragments were isolated using the QIAEX II Gel Extraction Kit (Qiagen, Valencia, CA) and purified using polyethylene glycol 6000 precipitation. PCR products were sequenced with the Big Dye Terminator Cycle Sequencing Kit V1.1 and analyzed with the ABI PRISM 310 Genetic Analyzer (Life Technologies, Carlsbad, CA). We also performed G-banded chromosome analysis at a resolution of 400–550 bands, genome-wide subtelomere fluorescence in situ hybridization (FISH) analysis, and array comparative genomic hybridization (array CGH) using Whole Human Genome Oligo Microarray Kits 244K (Agilent Technologies Inc., Palo Alto, CA) to identify genomic abnormalities.

RESULTS

G-banded chromosome analysis and genome-wide subtelomere FISH analyses did not show chromosomal rearrangements in the patient. Array CGH analysis did not show copy number changes in the patient's genome with the exception of known copy-number variations (CNVs). Since some patients with IFAP syndrome have been reported to present with several clinical features of BRESEK/BRESHECK syndrome, including severe intellectual disability, vertebral and renal anomalies, and Hirschsprung disease, we conducted a comprehensive sequencing analysis of all exons and intron–exon boundaries of *MBTPS2*. This analysis identified a missense mutation (c.1286G>A, [p.Arg429His]) in exon 10, which was previously reported for IFAP syndrome (Fig. 3). The mutation was also found in one allele of the mother (I-2), indicating that the mutation was of maternal origin and that the mother was a heterozygous carrier (Fig. 3).

DISCUSSION

In this report, we describe the fourth male patient with BRESHECK syndrome in whom we identified a missense mutation (c.1286G>A, [p.Arg429His]) in *MBTPS2*, which is the causal gene for IFAP syndrome. *MBTPS2* encodes a membrane-embedded zinc metalloprotease, termed site-2 protease (S2P). S2P cleaves and activates cytosolic fragments of sterol regulatory element binding proteins (SREBP1 and SREBP2) and a family of bZIP membrane-bound transcription factors of endoplasmic reticulum (ER) stress sensors (ATF6, OASIS), after a first luminal proteolytic cut by site-1 protease (S1P) within Golgi membranes [Sakai et al., 1996; Ye et al., 2000; Kondo et al., 2005; Asada et al., 2011]. The SREBPs control the expression of many genes involved in the biosynthesis and uptake of cholesterol, whereas ATF6 and OASIS induce many genes that clean up accumulated unfolded proteins in the ER. Dysregulated SREBP activation, impaired lipid metabolism, and accumulation of unfolded proteins in the ER caused by *MBTPS2* mutations could lead to disturbed differentiation of epidermal structures, resulting in the symptom triad of IFAP syndrome [Cursiefen et al., 1999; Traboulsi et al., 2004; Elias et al., 2008]. Oeffner et al. [2009] first identified five missense mutations in *MBTPS2* in patients with IFAP

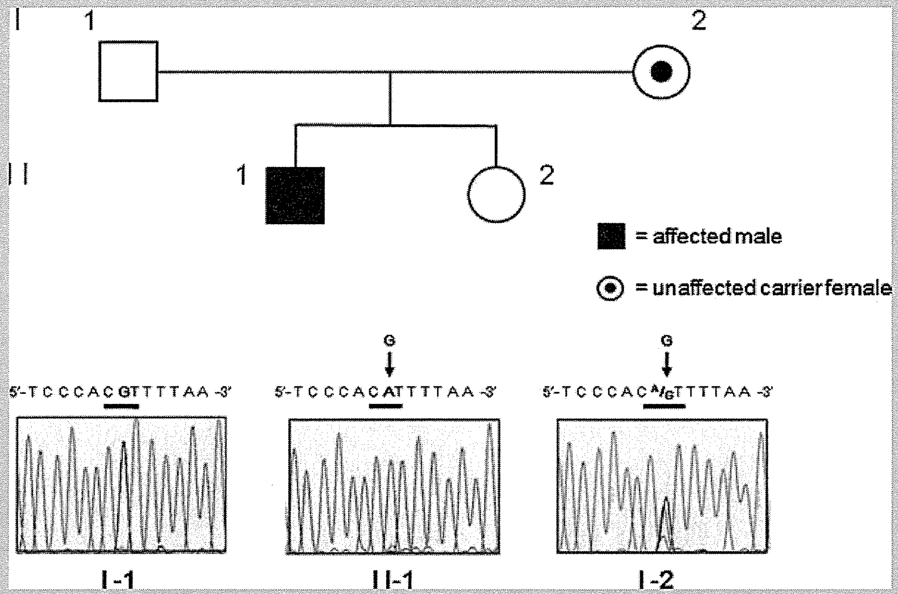
I
1
2
II
1
2
= affected male
= unaffected carrier female
G
G
5'-T C C C A C GT T T T A A -3'
5'-T C C C A C AT T T T A A -3'
5'-T C C C A C $^A/_G$T T T T A A -3'
I-1
II-1
I-2

FIG. 3. Identification of a disease mutation. The sequence analyses of the patient (II-1) showed a c.1286G>A variant in exon 10 of *MBTPS2*, which predicts p.Arg429His, as indicated by the arrow (middle panel). The mother (I-2) was heterozygous for the mutation ($C^A/_GT$) (right panel).

syndrome. Transfection studies using wild type and mutant *MBTPS2* expression constructs demonstrated that the five *MBTPS2* mutations did not affect S2P protein amount and localization in the ER. However, enzyme activities, as measured by sterol responsiveness, were decreased in S2P-deficient M19 cells when the mutant *MBTPS2* was transiently expressed. Interfamilial phenotypic differences between male IFAP patients and the properties of mutants in functional assays predict a genotype–phenotype correlation, ranging from mild forms of the triad with relatively high enzyme activity (~80%) to severe manifestations of intellectual disability, various developmental defects, and early death with low enzyme activity (~15%). The identified p.Arg429His mutation in the patient reported here is one of the five missense mutations with the lowest enzyme activity. It was previously reported that all four patients harboring the p.Arg429His mutation died within 14 months of birth. The five mutations were not located in the HEIGH motif (amino acids [aa] 171–175) or in the $LD_{467}G$ sequence, both of which are regions important for coordinating the zinc atom at the enzymatic active site for protease activity in the Golgi membrane [Zelenski et al., 1999]. However, among the five mutations, the p.Arg429His mutation is located closest to the intramembranous domain, and it strongly reduced the enzymatic activity and caused a severe phenotype. This finding suggests that mutations in the HEIGH motif or in the $LD_{467}G$ sequence are fatal because they lead to a null function of the S2P. Although the detailed skin findings of the four patients with the p.Arg429His mutation have not been reported, it should be noted that one of the four patients (3-III:4) with the p.Arg429His mutation had brain anomaly, seizures, psychomotor retardation, vertebrae anomaly, Hirschsprung disease, absence of a kidney, atrial septum defect, and inguinal hernia, in addition to the symptom triad of IFAP syndrome [Oeffner et al., 2009]. These symptoms overlap with the majority of symptoms observed in BRESHECK syndrome (BRESHK; six of eight symptoms observed in BRESHECK) (Table I), and the present patient has BRESHECK syndrome. Collectively, these observations suggest that the most severe form of the syndrome caused by the p.Arg429His mutation in *MBTPS2* shows features quite similar or identical to those of BRESEK/BRESHECK syndrome.

There are two major differences in the definitions of IFAP syndrome and BRESEK/BRESHECK syndrome. Ichthyosis follicularis, one of the triad symptoms of IFAP syndrome, is a clinical condition of the skin. However, several studies on IFAP syndrome have reported various skin eruptions such as psoriasis-like and ichthyosis-like eruptions [Martino et al., 1992; Sato-Matsumura et al., 2000]. In contrast, patients with BRESEK/BRESHECK syndrome showed severe lamellar desquamation with diffuse scaling [Reish et al., 1997], similar to that observed in the present patient. This could be because of the difference in features of the skin, namely, ichthyosiform erythroderma-like appearance versus ichthyosis follicularis, in patients with the most severe forms of *MBTPS2* mutation and patients with IFAP syndrome who were described earlier, respectively.

The second difference is that photophobia was not described in the reported three male patients with BRESEK/BRESHECK syndrome [Reish et al., 1997; Tumialán and Mapstone, 2006]. In the present patient, photophobia became evident after he was diagnosed with BRESHECK syndrome. Photophobia is a symptom of epithelial disturbances of the cornea, such as ulceration and vascularization, which result in corneal scarring [Traboulsi et al., 2004]. In the most severe cases of *MBTPS2* mutation, such as patients with severe intellectual disability who are bedridden and die early, it is likely that the patients were treated in the hospital without being exposed to sunlight. Therefore, it would be difficult to observe photophobia as a main symptom in those cases. Moreover, two previously described patients with BRESEK/BRESHECK syndrome had initial maldevelopment of one eye or small optic nerves. In these patients, photophobia may not have been obvious because of malformations of the eyes and optic nerves [Reish et al., 1997]. In our study, the patient showed clinical features of BRESHECK syndrome and photophobia with *MBTPS2* mutation, indicating that the clinical features of the present patient are extremely broad compared to the features of IFAP syndrome caused by *MBTPS2* mutation that have been previously reported [MacLeod, 1909].

Recently, a missense mutation (c.1523A>G, [p.Asn508Ser]) in *MBTPS2* was identified from 26 cases of three independent families with keratosis follicularis spinulosa decalvans (KFSD; OMIM# 308800), which is characterized by the development of hyperkeratotic follicular papules on the scalp followed by progressive alopecia of the scalp, eyelashes, and eyebrows in addition to childhood photophobia and corneal dystrophy [Aten et al., 2010]. A significant association was found between KFSD and the p.Asn508Ser mutation. The specific localization of alopecia to the scalp, eyelashes, and eyebrows and the limited childhood photophobia of KFSD indicate that KFSD has a relatively mild phenotype. The authors postulate that IFAP syndrome and KFSD are within the spectrum of one genetic disorder with a partially overlapping phenotype and propose that a new name should be chosen for KFSD/IFAP syndrome with an *MBTPS2* mutation. In contrast, the BRESHECK syndrome observed in the present patient has a severe phenotype caused by the p.Arg429His mutation. The present patient and the two patients (3-III:3 and 3-III:4) with the p.Arg429His mutation displayed broader clinical features, including eight features (BRESHECK) and six features (RESHCK and BRESHK) of BRESEK/BRESHECK syndrome, respectively (patients 4, 6, and 7; Table I) [Oeffner et al., 2009]. There is a debate regarding whether the two patients harboring six features were correctly diagnosed with BRESEK/BRESHECK syndrome since the patients did not have "BRESEK" but rather a combination of six other clinical features. To better understand and clearly distinguish the clinical features of the present patient from those of the reported patients with *MBTPS2* mutations, we propose the nomenclature of "BRESHECK/IFAP syndrome" for the present patient because he has clinical features of BRESHECK syndrome. We also suggest that the BRESHECK/IFAP syndrome be used for a broader definition that would include patients harboring most features of BRESHECK syndrome, including the previously reported two patients (3-III:3 and 3-III:4) with p.Arg429His mutation in *MBTPS2* [Oeffner et al., 2009]. Data from further genetic and clinical studies on more patients are required to determine which genes or *MBTPS2* mutations are associated with BRESEK/BRESHECK or BRESHECK/IFAP syndrome, respectively.

ACKNOWLEDGMENTS

We thank the patient and his family for participating in the study. This study was supported by the Takeda Science Foundation (to N.W.) and by the Health Labour Sciences Research Grant (to S.M. and N.W.).

REFERENCES

Aten E, Brasz LC, Bornholdt D, Hooijkaas IB, Porteous ME, Sybert VP, Vermeer MH, Vossen RH, van der Wielen MJ, Bakker E, Breuning MH, Grzeschik KH, Oosterwijk JC, den Dunnen JT. 2010. Keratosis follicularis spinulosa decalvans is caused by mutations in MBTPS2. Hum Mutat 31:1125–1133.

Asada R, Kanemoto S, Kondo S, Saito A, Imaizumi K. 2011. The signalling from endoplasmic reticulum-resident bZIP transcription factors involved in diverse cellular physiology. J Biochem 149:507–518.

Cursiefen C, Schlötzer-Schrehardt U, Holbach LM, Pfeiffer RA, Naumann GOH. 1999. Ocular findings in ichthyosis follicularis, atrichia, and photophobia syndrome. Arch Ophthalmol 117:681–684.

Elias PM, Williams ML, Holleran WM, Jiang YJ, Schmuth M. 2008. Pathogenesis of permeability barrier abnormalities in the ichthyoses: Inherited disorders of lipid metabolism. J Lipid Res 49:697–714.

Kondo S, Murakami T, Tatsumi K, Ogata M, Kanemoto S, Otori K, Iseki K, Wanaka A, Imaizumi K. 2005. OASIS, a CREB/ATF-family member, modulates UPR signalling in astrocytes. Nat Cell Biol 7:186–194.

MacLeod JMH. 1909. Three cases of 'ichthyosis follicularis' associated with baldness. Br J Dermatol 21:165–189.

Martino F, D'Eufemia P, Pergola MS, Finocchiaro R, Celli M, Giampà G, Frontali M, Giardini O. 1992. Child with manifestations of dermotrichic syndrome and ichthyosis follicularis alopecia photophobia (IFAP) syndrome. Am J Med Genet 44:233–236.

Oeffner F, Fischer G, Happle R, König A, Betz RC, Bornholdt D, Neidel U, Boente Mdel C, Redler S, Romero-Gomez J, Salhi A, Vera-Casaño A, Weirich C, Grzeschik KH. 2009. IFAP syndrome is caused by deficiency in MBTPS2, an intramembrane zinc metalloprotease essential for cholesterol homeostasis and ER stress response. Am J Hum Genet 84:459–467.

Reish O, Gorlin RJ, Hordinsky M, Rest EB, Burke B, Berry SA. 1997. Brain anomalies, retardation of mentality and growth, ectodermal dysplasia, skeletal malformations, Hirschsprung disease, ear deformity and deafness, eye hypoplasia, cleft palate, cryptorchidism, and kidney dysplasia/hypoplasia (BRESEK/BRESHECK): New X-linked syndrome? Am J Med Genet 68:386–390.

Sakai J, Duncan EA, Rawson RB, Hua X, Brown MS, Goldstein JL. 1996. Sterol-regulated release of SREBP-2 from cell membranes requires two sequential cleavages, one within a transmembrane segment. Cell 85: 1037–1046.

Sato-Matsumura KC, Matsumura T, Kumakiri M, Hosokawa K, Nakamura H, Kobayashi H, Ohkawara A. 2000. Ichthyosis follicularis with alopecia and photophobia in a mother and daughter. Br J Dermatol 142:157–162.

Traboulsi E, Waked N, Mégarbané H, Mégarbané A. 2004. Ocular findings in ichthyosis follicularis–alopecia–photophobia (IFAP) syndrome. Ophthal Genet 25:153–156.

Tumialán LM, Mapstone TB. 2006. A rare cause of benign ventriculomegaly with associated syringomyelia: BRESEK/BRESHECK syndrome. Case illustration. J Neurosurg 105:155.

Ye J, Rawson RB, Komuro R, Chen X, Davé UP, Prywes R, Brown MS, Goldstein JL. 2000. ER stress induces cleavage of membrane-bound ATF6 by the same proteases that process SREBPs. Mol Cell 6:1355–1364.

Zelenski NG, Rawson RB, Brown MS, Goldstein JL. 1999. Membrane topology of S2P, a protein required for intramembranous cleavage of sterol regulatory element-binding proteins. J Biol Chem 274:21973–21980.